Available online at www.sciencedirect.com
SCIENCE DIRECT®
Electrochimica Acta 50 (2005) 1307–1315
ELECTROCHIMICA Acta
www.elsevier.com/locate/electacta

Transient analysis of polymer electrolyte fuel cells

Yun Wang, Chao-Yang Wang*

Department of Mechanical and Nuclear Engineering, Electrochemical Engine Center (ECEC), The Pennsylvania State University, University Park, PA 16802, USA

Received 17 May 2004; received in revised form 22 July 2004; accepted 14 August 2004
Available online 2 October 2004

Abstract

A three-dimensional, transient model has been developed to study the transient dynamics of polymer electrolyte fuel cell (PEFC) operation. First, various time constants are estimated for important transient phenomena of electrochemical double-layer discharging, gas transport through the gas diffusion layer (GDL) and membrane hydration. It is found that membrane hydration occurs over a period of 10 s, the gas transport of 0.01–0.1 s, with the double-layer discharging being negligibly fast. Subsequently, extensive numerical simulations, with the transient processes of membrane hydration and gas transport taken into consideration, are carried out to characterize the dynamic response of a singe-channel PEFC with N112 membrane. The results show that the time for fuel cells to reach steady state is in the order of 10 s due to the effect of water accumulation in the membrane, consistent with theoretical estimation. In addition, overshoot or undershoot of the current densities is found during the step changes in some operating conditions, and detailed results are provided to reveal the dynamic physics of these phenomena.

Keywords: Transient model; Polymer electrolyte fuel cell; Dynamic response; Overshoot; Undershoot; Membrane water uptake

1. Introduction

Due to the two major improvements of polymer electrolyte fuel cells (PEFC) technology, the development of perfluorosulfonic-acid membranes and dramatic reduction in catalyst loading, PEFCs have gained much attention over recent years, particularly for mobile applications [1]. A PEFC is composed of a membrane electrode assembly (MEA) covered by two gas diffusion layers (GDL) placed between two current collector plates. The plates normally are grooved with serpentine or interdigitated flow field, while the GDL is characterized as highly porous media allowing reactant transport and product removal between the gas channel and MEA. Electrochemical reactions occur in the catalyst layers, and the membrane, normally made up of Nafion®, plays the dual roles of gas separation and proton conduction.

The hydration of the membrane is critical to the performance of the PEFC because the proton conductivity of the membrane is strongly correlated with the water content defined as the number of water molecules per sulfonic acid group. High water content results in low internal resistance of the PEFC. Membrane dryout may occur due to water electro-osmotic drag or low humidity operation, which is preferred particularly in the automobile applications. On the other hand, too much water will cause flooding of the electrode, which prevents the access of the reactant gas to the catalyst and exacerbates the mass transport loss. Water management is still a central issue in PEFC technology.

Much has been done in the literature to numerically study water management in PEFCs. However, most of them were concerned only with the steady-state condition, while the dynamic behavior is of paramount importance to automotive PEFCs, given the rapid variation of loads in the application. Transient phenomena in PEFCs have been studied by several researchers. Amphlett et al. [2] presented an analytical model to study the dynamic responses of temperature and current during start-up, load step-up and shut-down for a PEFC stack. Their transient model only considered the time domain and was based on coupling the steady-state electrochemical

* Corresponding author. Tel.: +1 814 863 4762; fax: +1 814 863 4848.
E-mail address: cxw31@psu.edu (C.-Y. Wang).

0013-4686/$ – see front matter © 2004 Elsevier Ltd. All rights reserved.
doi:10.1016/j.electacta.2004.08.022

kinetic equation with an unsteady, lumped-parameter thermal model. Their subsequent work [3] experimentally studied the coupled system of a fuel cell stack and a lead–acid battery. An electric circuit, which included the ohmic resistance in the electrolyte and current collector, overvoltage due to diffusion, migration and charge transfer, and double-layer capacitance, was used to describe the response of the battery. The same circuit was adopted for the fuel cell stack. A methodology was presented to predict the response of this fuel cell/battery hybrid system under various loads. Ceraolo et al. [4] studied the static and dynamic behavior of PEFCs numerically. Their one-dimensional model only considered the cathode side, and the transient terms were added to the species balance and phase potential equation. Experiments were also performed to provide the model input parameters and to validate the simulation results. In general, these models were too simple to completely understand the intricate dynamics of PEFCs, particularly the governing fundamental processes.

On the other hand, several accurate steady-state models have been proposed in the open literature, which include a detailed description of the physico-chemical processes and couple the transport equations with electrochemical kinetics in PEFCs. Specially, the model of Dutta et al. [5,6] treats the MEA as an interface without thickness and ignores the membrane water storage capability; thus this model cannot be used to simulate transient phenomena. In contrast, the model of Wang and co-workers [7–11] includes the full description of water and proton co-transport in the three-dimensional MEA, thus it could provide detailed information of water behaviors in this vital component, such as water accumulation, which is essential to the transient study. The importance of water accumulation in the membrane on the PEFC transient behavior will be discussed in the following section. In addition, Um et al. [8] also performed a brief transient analysis, where the membrane remained fully hydrated and thus only the transient process of gas transport was captured.

The present study is to extend the single-domain model of Um et al. [7,8] by considering all the important transient processes occurring in the PEFC, such as gas transport, water accumulation in the membrane, and electrochemical double-layer discharge. A three-dimensional, transient, single-phase model is developed along with theoretical estimation of various time constants. The transient model is numerically implemented into Star-CD®, a commercial CFD software, based on its user coding capacity. Dynamic responses of a single-channel PEFC with N112 membrane are numerically explored under both humidified and dry cathode conditions.

2. Mathematical model

2.1. Governing equations

The basic transport equation for water-containing membrane can be stated as:

$$\varepsilon_{\mathrm{m}}\frac{\partial C_{\mathrm{w}}^{\mathrm{m}}}{\partial t} = \nabla\cdot(D_{\mathrm{w}}^{\mathrm{m^{eff}}}\nabla C_{\mathrm{w}}^{\mathrm{m}}) - \frac{1}{F}\nabla(n_{\mathrm{d}}i_{\mathrm{e}}) \tag{1}$$

where ε_{m} is the volume fraction of ionomer in the membrane and the last term on the right describes the electro-osmotic drag effect. Here, $C_{\mathrm{w}}^{\mathrm{m}}$ is the equivalent water concentration in the membrane defined as:

$$C_{\mathrm{w}}^{\mathrm{m}} = \frac{\rho\lambda}{\mathrm{EW}} \tag{2}$$

where ρ and EW are the density and equivalent molecular weight of the membrane, respectively. The water content, λ, is the number of water molecules per sulfonic acid group within the membrane. This is an important parameter on which proton conductivity and transport properties of the membrane are based, and can be calculated from [12]:

$$\lambda = \begin{cases} 0.043 + 17.81a - 39.85a^2 & \\ \quad +36.0a^3 & \text{for } 0 < a \le 1 \\ 14 + 1.4(a-1) & \text{for } 1 \le a \le 3 \end{cases} \tag{3}$$

where the water activity is defined as:

$$a = \frac{C_{\mathrm{w}}RT}{p^{\mathrm{sat}}} \tag{4}$$

Physically, Eq. (1) indicates that water accumulation in the membrane is balanced by the net flux of diffusion and electro-osmotic drag, given that the convection effect is ignored. Considering that a dry membrane is hydrated by product water generated at a constant current density of I, the time constant, τ_{m}, for membrane hydration can be estimated by equating the rate of water storage to that of water production. That is:

$$\tau_{\mathrm{m}} = \frac{(\rho\delta_{\mathrm{m}}\Delta\lambda)/\mathrm{EW}}{I/2F} \tag{5}$$

For Nafion® 112 at 30 °C, $\Delta\lambda$ = 14, and I = 1 A/cm^2, τ_{m} is about 25 s. This immediately points out the importance of the transient term in Eq. (1). Note that the time constant, τ_{m}, may vary with the temperature within the order of magnitude.

Within the catalyst layer, the conservation equation of water transport in the transient form then can be expressed as:

$$\varepsilon_{\mathrm{g}}\frac{\partial C_{\mathrm{w}}}{\partial t} + \varepsilon_{\mathrm{m}}\frac{\partial C_{\mathrm{w}}^{\mathrm{m}}}{\partial t} = \nabla\cdot(D_{\mathrm{w}}^{\mathrm{g^{eff}}}\nabla C_{\mathrm{w}}) + \nabla\cdot(D_{\mathrm{w}}^{\mathrm{m^{eff}}}\nabla C_{\mathrm{w}}^{\mathrm{m}}) - \frac{1}{F}\nabla\cdot(n_{\mathrm{d}}i_{\mathrm{e}}) \tag{6}$$

The two terms on the left hand represent the rate of water storage in the gas and membrane phases, respectively. Assuming thermodynamic equilibrium of water between the gas and membrane phases, the above equation can be rearranged as:

$$\varepsilon^{\mathrm{eff}}\frac{\partial C_{\mathrm{w}}}{\partial t} = \nabla\cdot(D_{\mathrm{w}}^{\mathrm{eff}}\nabla C_{\mathrm{w}}) - \frac{1}{F}\nabla\cdot(n_{\mathrm{d}}i_{\mathrm{e}}) \tag{7}$$

where the effective factor, ε^{eff}, is defined as:

$$\varepsilon^{\text{eff}} = \varepsilon_{\text{g}} + \varepsilon_{\text{m}} \frac{\mathrm{d}C_{\text{w}}^{\text{m}}}{\mathrm{d}C_{\text{w}}} = \varepsilon_{\text{g}} + \varepsilon_{\text{m}} \frac{1}{\text{EW}} \frac{RT}{p^{\text{sat}}} \left(\rho + \lambda \frac{\mathrm{d}\rho}{\mathrm{d}\lambda} \right) \frac{\mathrm{d}\lambda}{\mathrm{d}a} \tag{8}$$

For Nafion® 11-series membranes having EW of 1.1 kg/mol, and membrane density, ρ, of 1980 kg/m^3 at 80 °C, the effective factor, ε^{eff}, is in the order of 10^2 to 10^3 for water activity $a < 1$.

Another transient phenomenon in PEFCs is charging or discharging of the electrochemical double-layer. The double-layer occurs in a thin layer (of the order of nm) adjacent to the reaction interface and acts as a capacitor during transience. Similar to porous electrodes of batteries, the double-layer in the catalyst layer of a PEFC can be regarded as being in parallel to a charge transfer reaction resistor. The importance of the double-layer can be evaluated by its time constant [13]:

$$\tau_{\text{dl}} = \delta_{\text{CL}}^2 aC \left(\frac{1}{\kappa} + \frac{1}{\sigma} \right) \tag{9}$$

where the symbols are defined in Appendix A. Normally, the capacity, C, is around 20 μF/cm^2 and specific area, a, is about 10^3/cm. Thickness of the catalyst layer, δ_{CL}, is 10^{-3} cm, κ is around 0.1 S/cm and σ is about 50 S/cm, which lead to a time constant of 0.2 μs, sufficiently short to be safely ignored for automotive PEFCs.

On the other hand, the time constant for species transport (e.g. diffusion) can be easily estimated by the diffusion time, i.e.

$$\tau_k = \frac{\delta_{\text{GDL}}^2}{D_{\text{g}}^{\text{eff}}} \tag{10}$$

Using the parameters shown in Table 4 and $D_{\text{g}}^{\text{eff}}$ around 10^{-5} m^2/s in the porous GDL yields τ_k in the order of 0.01 s.

To summarize, the time constants of membrane hydration and gas transport are sufficiently long to be important in transient analyses of automotive PEFCs, whereas the time constant of the electrochemical double-layer is sufficiently short to be neglected. Consequently, the governing equations for a transport and electrochemical coupled PEFC model can be written in a single-domain form as follows:

$$\text{continuity}: \quad \nabla \cdot \vec{u} = 0 \tag{11}$$

$$\text{momentum}: \quad \frac{1}{\varepsilon} \left[\frac{\partial \vec{u}}{\partial t} + \frac{1}{\varepsilon} \nabla \cdot (\vec{u}\vec{u}) \right] = -\nabla \left(\frac{p}{\rho} \right) + \nabla \cdot \tau + S_u \tag{12}$$

$$\text{species}: \quad \varepsilon \frac{\partial C_k}{\partial t} + \nabla \cdot (\vec{u} C_k) = \nabla \cdot (D_k^{\text{eff}} \nabla C_k) + S_k \tag{13}$$

$$\text{charge}: \quad 0 = \nabla \cdot (\kappa^{\text{eff}} \nabla \Phi_{\text{e}}) + S_\Phi \tag{14}$$

Table 1
Source terms for the conservation equations in each region

	S_u	S_k	S_ϕ
Gas channels	0	0	–
Diffusion layers	$S_u = -\frac{\mu}{K}\vec{u}$	0	0
Catalyst layers	$S_u = -\frac{\mu}{K}\vec{u}$	$S_k = -\nabla \cdot \left(\frac{n_{\text{d}}}{F} i_{\text{e}} \right) - \frac{s_k j}{nF}$	$S_\phi = j$
Membrane	$S_u = -\frac{\mu}{K}\vec{u}$	0	0

Note: n_{d} is the electro-osmotic drag coefficient for water. For H_2 and O_2, $n_{\text{d}} = 0$.

where ε becomes unity in gas channels and a constant density is assumed in Eqs. (11) and (12). Moreover, Eq. (13) encompasses the water transport equations in the MEA, i.e. Eqs. (1) and (7). The various source term, S, and electrochemical and physical properties are listed in Tables 1–3, respectively. The present model is a transient extension of the previous model [7–11] based on molar concentration and assuming constant density and no mass source in the continuity and momentum equations. A more complete model without making these assumptions indicated an excellent applicability of the present model to the conditions under consideration [14].

2.2. Boundary and initial conditions

Eqs. (11)–(14), form a complete set of governing equations with eight unknowns: $\vec{u}$ (three components), P, C_{H_2}, C_{O_2}, $C_{\text{H}_2\text{O}}$ and ϕ_{e}. Their corresponding boundary and initial conditions are described as follows.

2.2.1. Flow inlet boundaries

The inlet velocity $\vec{u}_{\text{in}}$ in a gas channel is expressed by the respective stoichiometric flow ratio, i.e., ξ_{a} or ξ_{c}, defined at a reference current density, I_{ref}, as:

$$\xi_{\text{a}} = \frac{C_{\text{H}_2} \rho_{\text{a}} u_{\text{in,a}} A_{\text{a}}}{I_{\text{ref}} A/(2F)} \quad \text{and} \quad \xi_{\text{c}} = \frac{C_{\text{O}_2} \rho_{\text{c}} u_{\text{in,c}} A_{\text{c}}}{I_{\text{ref}} A/(4F)} \tag{15}$$

where A_{a} and A_{c} are the flow cross-sectional areas of the anode and cathode gas channels, respectively. The inlet molar concentrations are determined by the inlet pressure and humidity according to the ideal gas law.

2.2.2. Outlet boundaries

Fully developed or no-flux conditions are applied:

$$\frac{\partial \vec{u}}{\partial n} = 0, \qquad \frac{\partial C_k}{\partial n} = 0, \qquad \frac{\partial \phi_{\text{e}}}{\partial n} = 0 \tag{16}$$

2.2.3. Wall

No-slip and impermeable velocity condition and no-flux condition are applied:

$$\vec{u} = 0, \qquad \frac{\partial C_k}{\partial n} = 0, \qquad \frac{\partial P}{\partial n} = 0, \qquad \frac{\partial \phi_{\text{e}}}{\partial n} = 0 \tag{17}$$

2.2.4. Initial conditions

The initial conditions are either zero or steady-state field from a previous operating point.

Table 2
Electrochemical properties

Description	Anode	Cathode
Transfer current density, j	$ai_{0,a}\left(\frac{C_{H_2}}{C_{H_2,ref}}\right)^{1/2}\left(\frac{\alpha_a+\alpha_c}{RT}F\eta\right)$	$-ai_{0,c}\left(\frac{C_{O_2}}{C_{O_2,ref}}\right)e^{((-\alpha_c F/RT)\eta)}$
Surface overpotential, η	$\Phi_s - \Phi_e - U_o$ (with $\Phi_s = 0$)	$\Phi_s - \Phi_e - U_o$ (with $\Phi_s = V_{cell}$)
Equilibrium potential, U_o (V)	0	$1.23 - 0.9 \times 10^{-3}\,(T - 298)$
Exchange current density × reaction surface area, ai_0 (A/m^3)	1.0×10^9	10000
Transfer coefficient, α	$\alpha_a + \alpha_c = 2$	$\alpha_c = 1$

Table 3
Physical and transport properties

Quantity	Value	Reference
Water activity, a	$a = \frac{C_w RT}{p^{sat}}$ and $\log_{10} p^{sat} = -2.1794 + 0.02953(T - 273.15) - 9.1837 \times 10^{-5}(T - 273.15)^2 + 1.4454 \times 10^{-7}(T - 273.15)^3$	Springer et al. [12]
Ionic conductivity of membrane, κ	$(0.005139\lambda - 0.00326)\,e\left[1268\left(\frac{1}{303} - \frac{1}{T}\right)\right]$	Springer et al. [12]
H_2O diffusivity in membrane, D_w^m	$D_w^m = \begin{cases} 3.1 \times 10^{-3}\lambda(e^{0.28\lambda} - 1)\,e^{[-2346/T]} & \text{for } 0 < \lambda \le 3 \\ 4.17 \times 10^{-4}\lambda(1 + 161\,e^{-\lambda})\,e^{[-2346/T]} & \text{otherwise} \end{cases}$	Motupally et al. [16]
Electro-osmotic drag coefficient, n_d	$n_d = \begin{cases} 1.0 & \text{for } \lambda \le 14 \\ \frac{1.5}{8}(\lambda - 14) + 1.0 & \text{otherwise} \end{cases}$	Zawodzinski et al. [17]
Membrane density, ρ	$\rho = \frac{1.98 + 0.0324\lambda}{1 + 0.0648\lambda} \times 10^3$	West and Fuller [18]
H_2/O_2 diffusivity in membrane, $D_{H_2}^m/D_{O_2}^m$	$2.59 \times 10^{-6}/1.22 \times 10^{-6}$	Bernardi and Verbrugge [19]
Gas diffusion coefficient in porous media, D^{eff}	$D^{eff} = \varepsilon^{1.5} D$	–
Diffusivity in the gas channels, D	$D_o\left(\frac{T}{353}\right)^{3/2}\left(\frac{1}{p}\right)$	Bird et al. [20]
Viscosity of anode/cathode gas, μ	$\mu = 9.88 \times 10^{-6} X_{H_2} + 1.12 \times 10^{-5} X_{H_2O} + 2.01 \times 10^{-5} X_{N_2} + 2.3 \times 10^{-5} X_{O_2}$	Incropera and DeWitt [21]

2.3. Numerical procedures

The conservation equations are solved by Star-CD® software with PISO algorithm, the pressure implicit splitting of operators [15]. PISO is based on predictor–corrector splitting for unsteady problems. The source terms and physical properties are incorporated in the user code. The mesh of a PEFC with a single channel is shown in Fig. 1. The geometry and physical parameters are listed in Table 4. To accurately describe water accumulation in the membrane, 10 grids are used within the membrane and 6 grids are placed in the catalyst layer in the through-plane direction. About 100,000 computational cells are used to capture the three-dimensional electrochemical and physical phenomena in the PEFC. Adaptive time stepping is used in which the current time step is inversely proportional to the temporal gradient of current density at the previous time step with the maximum of 0.1 s. A total of 500 iterations is sufficient for one transient case, which takes less than 1 h on an Intel® Xeon™ Processor 2.0 GHz.

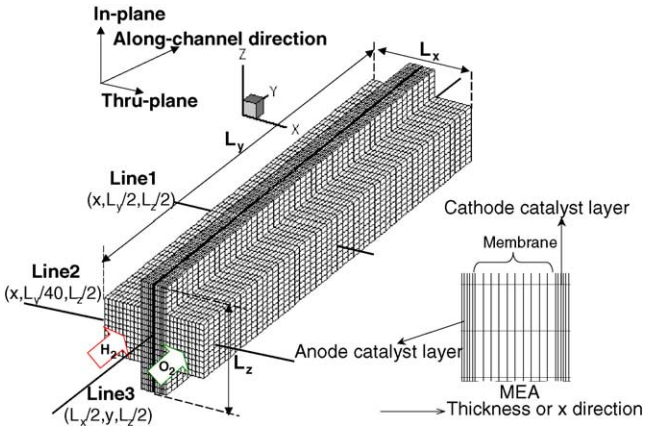

Fig. 1. The details of computational domain and mesh of the single-channel PEFC. Lines 1–3 are the three typical positions chosen to display detailed results.

3. Results and discussion

A single-channel PEFC with Nafion® 112 membrane is chosen for a parametric study. While the focus of the

Table 4
Geometrical and physical parameters

Quantity	Value
Gas channel depth/width (mm)	1.0/1.0
Shoulder width (mm)	1.00
Diffusion layer thickness, δ_{GDL} (mm)	0.3
Catalyst layer thickness, δ_{CL} (mm)	0.01
Membrane (N112) thickness, δ_m (mm)	0.051
Fuel cell height/length (mm)	2.0/100.0
Anode/cathode pressures, P (atm)	2.0/2.0
Stoichiometric flow ratio ξ in anode/cathode	2.0/2.0
Temperature of fuel cell (K)	353
Porosity of diffusion layers, ε	0.6
Porosity of catalyst layers, ε_g	0.4
Volume fraction of ionomer in catalyst layers, ε_m	0.26
Permeability of diffusion layers, K (m^2)	10^{-12}
H_2 diffusivity in anode gas channel at standard condition, $D_{o,H_2,a}$ (m^2/s)	1.1028×10^{-4}
H_2O diffusivity in anode gas channel at standard condition, $D_{o,w,a}$ (m^2/s)	1.1028×10^{-4}
O_2 diffusivity in cathode gas channel at standard condition, $D_{o,O_2,c}$ (m^2/s)	3.2348×10^{-5}
H_2O diffusivity in cathode gas channel at standard condition, $D_{o,w,c}$ (m^2/s)	7.35×10^{-5}

present work is on elucidating dynamic behaviors under low-humidity operation, a fully humidified case is also simulated for comparison as this case features the transience of gas transport only with the transient process of membrane hydration (remains always hydrated) becoming irrelevant. All results are intended to explore the transient response to a step change from one steady-state operating point to another. The two types of step change studied are in the cell voltage and cathode inlet relative humidity.

Fig. 2 shows dynamic responses of average current densities to the step change of cathode inlet humidification from RH = 0% to 100% under various cell voltages. The humidity step change occurs at t = 0 from the steady state of RHa/c = 100/0%. It is seen that it takes approximately 20 s for the fuel cell to reach the new steady state, in accordance with the time constant of membrane water uptake estimated by Eq. (5). In addition, the transition period under higher cell voltage is slightly longer because lower current density in this condition results in less water production, making it longer to hydrate the membrane. In addition, despite that humidified air stream contains less oxygen, the current density continues to increase in the transition process, which demonstrates that the ohmic resistance, controlled by water content in the membrane, dominates the PEFC performance.

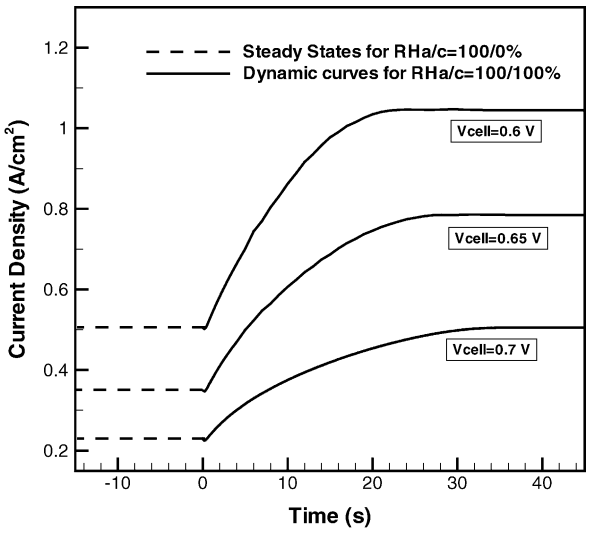

Fig. 2. Dynamic responses of average current density to the step change of the cathode inlet humidification from RH = 0% to 100%, under 0.6, 0.65 and 0.7 V.

It is of interest to compare water uptake by the membrane to that by the reactant gases within the PEFC. This ratio can be estimated by:

$$\frac{\varepsilon^{\text{eff}} V_m}{V_{a,ch} + V_{c,ch}} \tag{18}$$

where V_m, $V_{a,ch}$ and $V_{c,ch}$ are the volumes of the membrane, anode gas channel and cathode gas channels, respectively. Fig. 3 shows the contour of ε^{eff} in the membrane under the steady state of V_{cell} = 0.65 V and RHa/c = 100/0%. It can be seen that ε^{eff} varies from 10^2 to 10^3. Noting that the depth of gas channels is usually 10–100 times the membrane thickness, Eq. (18) indicates that the membrane holds 10–10^2 times more water than the reactant gases. Thus, membrane water is the most important part in the transient process of water management.

Fig. 4 shows the evolution of water concentration profiles in the fuel cell cross-section at the mid-length, i.e. along Line 1 (x, L_y/2, L_z/2) (see Fig. 1), when the inlet cathode humidity is switched from 0% to 100% under 0.65 V. It can be seen that the transition time is of the same order as the one shown in Fig. 2. Interestingly, it is shown that in 0.1 s after the switch, water concentration changes much in the cathode side while there is nearly no change occurring in the anode side. This can be explained by the time for species to be convected down the channel, namely L_y/u_y. Given u_y = 1.0 m/s at the cathode side

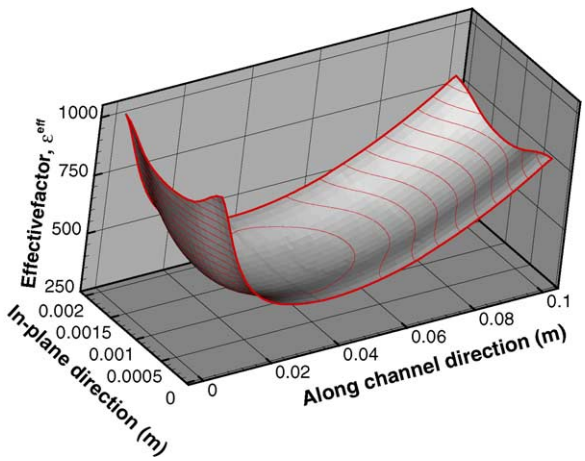

Fig. 3. The effective factor, ε^{eff}, in Eq. (8) in the middle of the membrane, under 0.65 V and RHa/c = 100/0%.

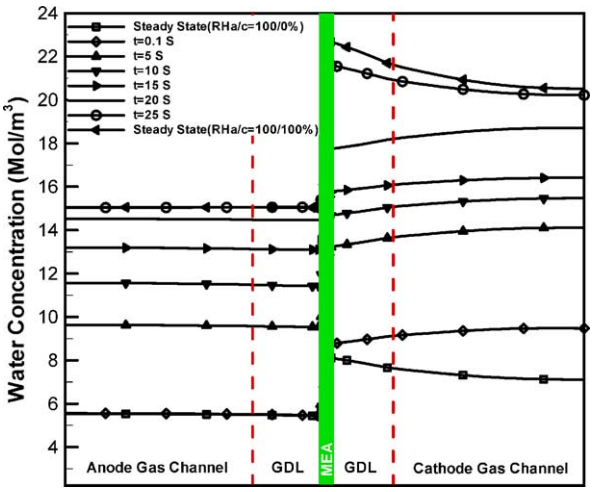

Fig. 4. Evolution of water concentration profiles along Line 1 (x, $L_y/2$, $L_z/2$), when the cathode inlet humidification changes from RH = 0% to 100% under 0.65 V.

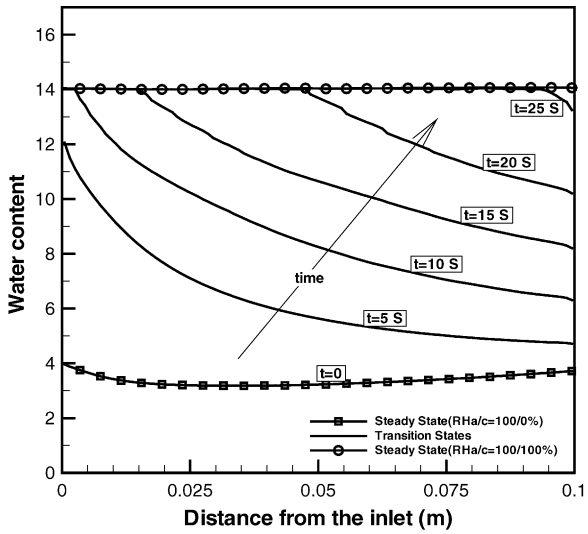

Fig. 5. Evolution of water content profiles along Line 3 ($L_x/2$, y, $L_z/2$), when the cathode inlet humidification changes from RH = 0% to 100% under 0.65 V.

and L_y =0.1 m, τ_k is in the order of 0.1 s. However, it takes about 15 s for the cathode gas on the middle plane to reach the inlet value, 15.9 mol/m^3, instead of 0.1 s. This is due to the quick species transport in the through-plane direction across the GDL, as indicated by Eq. (10), making the cathode wet inlet stream lose water to the dry membrane for the initial period.

Evolution of the water concentration profiles in the cathode GDL shown in Fig. 4 is of interest to note. At t = 0, the gas in the cathode channel is relatively dry and the product water generated in the cathode catalyst layer is removed to the channel, thus a water concentration gradient is directed from the catalyst layer/GDL interface to the GDL/channel one. However, once the inlet instantly switches to the fully humidified state, the high humidification front propagates into the middle of the gas channel, altering the water concentration gradient to go from the GDL/channel interface to the catalyst layer/GDL one. This means that the membrane takes up water not only from ORR production but also from the humidified gas stream in the channel. The consequent rise in the membrane water content then gives rise to a higher current density and hence more water production under the same cell voltage. Further increase in the membrane hydration will finally make the product water removed to the cathode gas stream, changing the water concentration gradient in GDL back to the initial shape.

Fig. 4 also shows that the water concentration profile on the anode side is altered by the change in the inlet humidity condition on the cathode. This is illustrative of the important role of water back diffusion through the membrane, which depends on the relative humidity difference between the cathode and anode.

The increase in anode water concentration with time can be readily explained by Fig. 5. Fig. 5 shows evolution of water content profiles along Line 3 ($L_x/2$, y, $L_z/2$), when inlet cathode humidification changes from 0% to 100% under 0.65 V. It is seen that the water content reaches the steady state first near to the flow inlet. After the membrane in the inlet area reaches full humidification within 10 s, it takes additional 15 s for the membrane in the outlet area to be fully hydrated.

Fig. 6 shows the dynamic responses of the average current density to the reverse step change in cathode inlet humidification from 100% to 0%, again under 0.6, 0.65 and 0.7 V cell voltages. First, it is seen that the transition occurs within about 40 s, while remaining on the same order of magnitude as theoretical time constant estimated by Eq. (5), it is twice longer than the reverse transition shown in Fig. 2. This is clearly indicative of a hysteretic effect that it takes longer for a fully hydrated membrane generating high current density to be de-hydrated by dry cathode gas. Second,

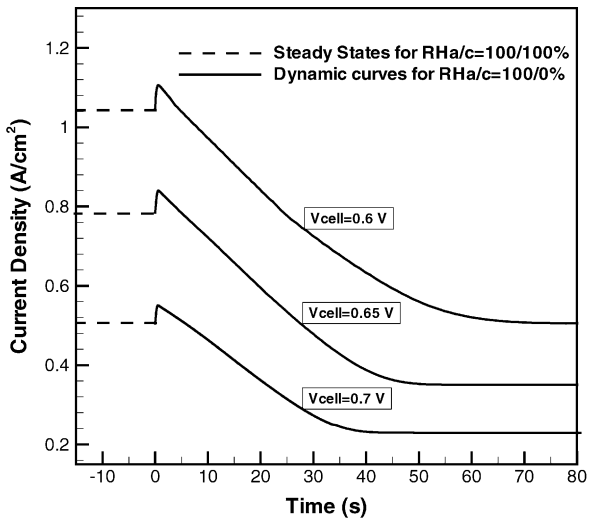

Fig. 6. Dynamic responses of average current density to the step change of the cathode inlet humidification from RH = 100% to 0%, under 0.6, 0.65 and 0.7 V.

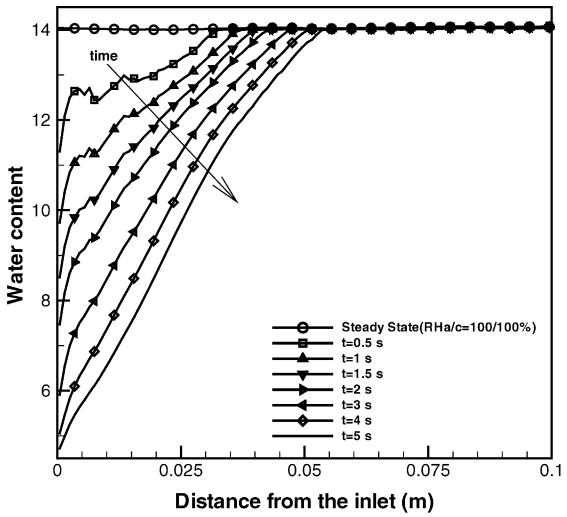

Fig. 7. Evolution of water content profiles along Line 3 ($L_x/2$, y, $L_z/2$), when the cathode inlet humidification changes from RH = 100% to 0% under 0.65 V.

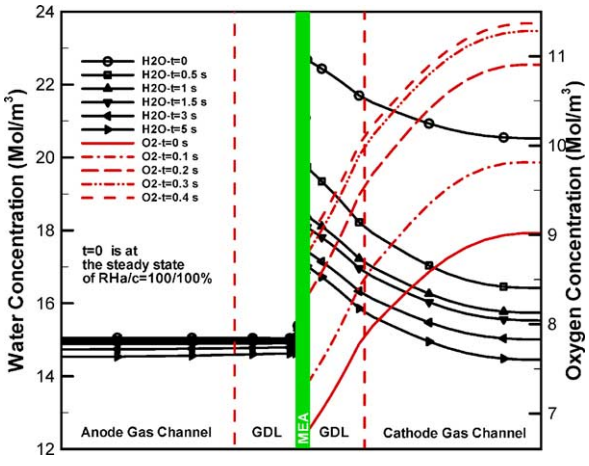

Fig. 8. Evolution of water and oxygen concentration profiles along Line 1 (x, $L_y/2$, $L_z/2$), when the cathode inlet humidification changes from RH = 100% to 0% under 0.65 V.

there exist obvious overshoots because the membrane is still hydrated and exhibits low ohmic resistance but the catalyst layer is already experienced with enriched oxygen supplied by the dry cathode gas. After the overshoots, current densities steadily decrease to their steady-state values as a result of membrane water reduction. In addition, contrary to the reverse case shown in Fig. 2, the time required to reach the steady state is shorter for the higher cell voltages. This can be explained by the fact that more water produced in the PEFC needs to be removed under lower cell voltages.

Fig. 7 presents the evolution of the water content profiles in the middle of the membrane during the first several seconds when overshoots occur. It is seen that water content in the membrane around the inlet area responds quickly to the step change in cathode gas humidification, similar to the result shown in Fig. 5. In addition, water content maintains fully hydrated level at most part of the membrane during the first 0.5 s, and even after 5 s, nearly half of the membrane is still fully hydrated.

Fig. 8 presents the evolutions of water and oxygen concentration profiles at the mid-length of the cell, showing that the water concentration is substantially reduced in the cathode side, while there is little change in the anode during the first 5 s. However, the gas in the cathode side still remains nearly fully humidified (i.e. C_{sat} = 15.9 mol/m^3) during this period. Meanwhile, the oxygen concentration increases significantly in 0.1 s due to the injection of dry, undiluted gas into the cathode. This result confirms the phenomenon of initial overshoot in the current density explained earlier.

Fig. 9 presents the dynamic responses of the average current density to a step change in cell voltages comparing a fully humidified case (i.e. RHa/c = 100/100%) with a dry cathode case (i.e. RHa/c = 100/0%). Times for onset of step changes are chosen arbitrarily to set apart the two response curves. For the fully humidified case, only the transience of reactant transport to the catalyst layer to meet the demand of reaction rate is operational. Thus, only the undershoot discovered previously by Um et al. [8] is seen, which is characteristic of low oxygen concentration at catalyst sites under lower cell voltage or high current density. The most part of undershoot occurs in a fraction of a second, consistent with the time constant of species diffusion. In contrast, for the dry condition, current density undergoes an undershoot followed by an overshoot. The overshoot, similarly to the ones in Fig. 6, can be explained by the fact that response of membrane hydration lags the one of oxygen transport in the cell. Also, the transition between the two steady states corresponding to the two cell voltages takes about 10 s, indicative of the dominance of membrane uptake phenomenon in the cell dynamic response.

Focusing on the first second after the step change in cell voltages, Fig. 10 shows the evolution of oxygen concentration profiles along Line 1 (x, $L_y/2$, $L_z/2$) and Line 2 (x, $L_y/40$,

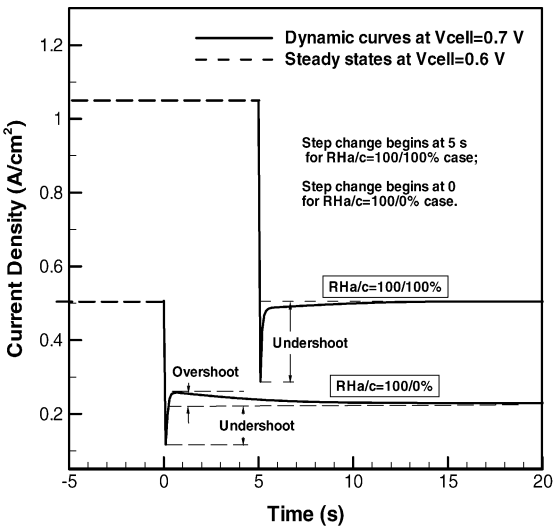

Fig. 9. Dynamic responses of average current density to the step change of cell voltages from 0.6 to 0.7 V, under RHa/c = 100/100% and 100/0%.

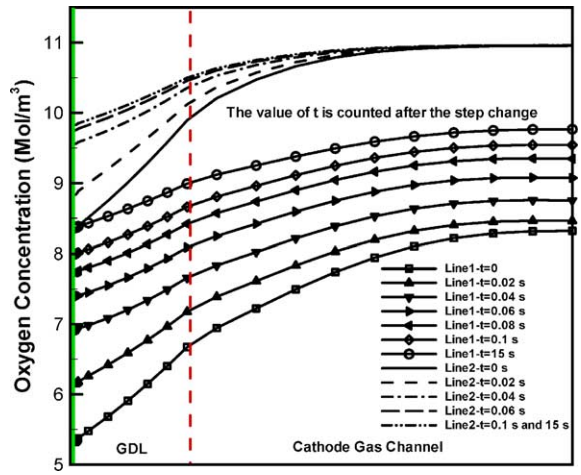

Fig. 10. Evolution of oxygen concentration profiles along Line 1 (x, $L_y/2$, $L_z/2$) and Line 2 (x, $L_y/40$, $L_z/2$), when cell voltages change from 0.6 to 0.7 V, under RHa/c = 100/100%.

$L_z/2$). In the inlet area, i.e. Line 2, it takes about 0.1 s for the oxygen concentration in the gas diffusion layer to increase to its steady state. At the mid-length of the cell, i.e. Line 1, longer time is needed due to the influence from the upstream.

Fig. 11 presents the dynamic responses of the average current density to the reverse change in cell voltages from 0.7 V back to 0.6 V again, considering two cases: RHa/c = 100/100% and 100/0%. Similar to Fig. 9, the transition takes around 10 s, and the curve jumps immediately after the step change, then gradually gets to its steady state in the fully humidified case. Overshoot occurs only in the full humidification case. Similar to the undershoot revealed in Fig. 9, the overshoot is characteristic of high oxygen concentration at catalyst sites under low current density. In contrast, in the dry cathode case, the hydration level of the membrane plays a more dominant role in the cell performance. More water production continues to enhance the cell performance after the pumping effect of high oxygen concentration under low current density, thus there exists no overshoot in this situation.

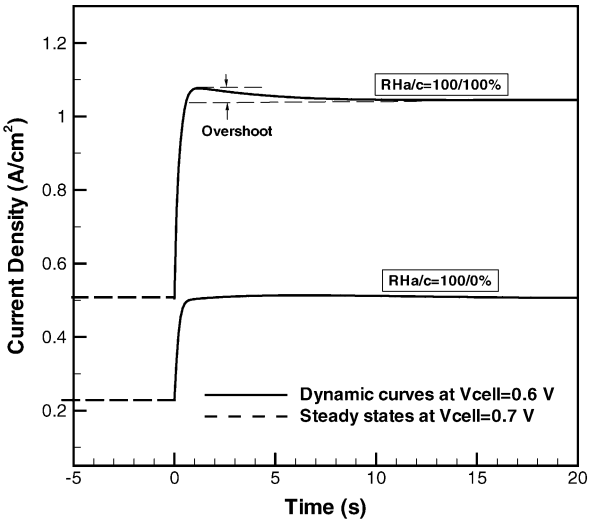

Fig. 11. Dynamic responses of average current density to the step change of cell voltages from 0.7 to 0.6 V, under RHa/c = 100/100% and 100/0%.

4. Conclusions

A transient model of PEFCs has been presented to study the intricate dynamic response to step changes in operating conditions. Time constants for electrochemical double-layer, gas transport, and water accumulation in the membrane were estimated to identify the dominant effects of membrane water uptake and gas transport processes on the transient performance of PEFCs. Numerical simulations were carried out to study the transience of a singe-channel PEFC with N112 membrane. Results indicate that after the step change, the transition takes place in the order of 10 s, and the membrane hydration was the controlling process in the transient analyses. In addition, overshoot or undershoot in the current density was found in certain cases. Detailed species distributions within the cell were provided to explain the physics underlying the transient phenomena and to indicate that under low-humidity operation membrane water accumulation is responsible, while under high-humidity operation oxygen transport dictates the dynamic response of PEFCs. The dynamic behaviors of PEFCs captured herein for the first time, including undershoot and overshoot in the current output, are expected to be useful for the design of power electronics and control algorithms for fuel cell engines.

Acknowledgement

Support for this work by Department of Energy and ConocoPhillips under cooperative agreement #DE-FC26-01NT41098 is acknowledged.

Appendix A. Nomenclature

a	water activity or effective catalyst area per unit volume (m^2/m^3)
A	superficial electrode area (m^2)
C	capacitance of the double-layer (mF/cm^2)
C_k	molar concentration of species k (mol/m^3)
D	mass diffusivity of species (m^2/s)
EW	equivalent weight of dry membrane (kg/mol)
F	Faraday's constant (96,487 C/equivalent)
i_e	superficial current density (A/m^2)
i_0	exchange current density (A/m^2)
I	current density (A/cm^2)
j	transfer current (A/cm^3)
K	permeability (m^2)
n	the direction normal to a surface
n_d	electro-osmotic drag coefficient (H_2O/H^+)

P	pressure (Pa)
R	gas constant (8.134 J/mol K)
RH	relative humidification
S	source term in transport equations
t	time (s)
T	temperature (K)
$\vec{u}$	velocity vector (m/s)
V_{cell}	cell potential (V)
X	mole fraction

Greek letters

α	transfer coefficient
δ	thickness (m)
ε	porosity
η	surface overpotential (V)
κ	ionic conductivity (S/m)
λ	membrane water content
μ	viscosity (kg/m s)
ξ	stoichiometric flow ratio
ρ	density (kg/m^3)
σ	electronic conductivity (S/cm)
τ	shear stress (N/m^2); time constant (s)
ϕ	phase potential (V)

Subscripts and superscripts

a	anode
c	cathode
ch	channel
CL	catalyst layer
dl	double-layer
e	electrolyte
eff	effective value
g	gas phase
GDL	gas diffusion layer
in	inlet
k	species
m	membrane phase; membrane
o	standard condition, 273.15 K and 101.3 kPa (1 atm)
ref	reference
s	solid phase of electrode
sat	saturate value
w	water

References

[1] M.L. Perry, T.F. Fuller, J. Electrochem. Soc. 149 (7) (2002) 59.
[2] J.C. Amphlett, R.F. Mann, B.A. Peppley, P.R. Roberge, A. Rodrigues, J. Power Sources 61 (1996) 183.
[3] J.C. Amphlett, E.H. de Olivera, R.F. Mann, P.R. Roberge, A. Rodrigues, J.P. Salvador, J. Power Sources 65 (1997) 173.
[4] M. Ceraolo, C. Miulli, A. Pozio, J. Power Sources 113 (2003) 131.
[5] S. Dutta, S. Shimpalee, J.W. Van Zee, Int. J. Heat Mass Transfer 44 (2001) 2029.
[6] S. Dutta, S. Shimpalee, J.W. Van Zee, J. Appl. Electrochem. 30 (2000) 135.
[7] S. Um, C.Y. Wang, Proceedings of the ASME IMECE, vol. 1, Orlando, FL, 2000, p. 19.
[8] S. Um, C.Y. Wang, K.S. Chen, J. Electrochem. Soc. 147 (2000) 4485.
[9] S. Um, C.Y. Wang, J. Power Sources 125 (2004) 40.
[10] H. Meng, C.Y. Wang, Chem. Eng. Sci. 59 (2004) 3331.
[11] H. Meng, C.Y. Wang, J. Electrochem. Soc. 151 (2004) A358.
[12] T.E. Springer, T.A. Zawodinski, S. Gottesfeld, J. Electrochem. Soc. 126 (1991) 2334.
[13] I.J. Ong, J. Newman, J. Electrochem. Soc. 146 (12) (1999) 4360.
[14] Y. Wang, C.Y. Wang, J. Electrochem. Soc., in press.
[15] R.I. Issa, J. Comp. Phys. 62 (1986) 40.
[16] S. Motupally, A.J. Becker, J.W. Weidner, J. Electrochem. Soc. 147 (2000) 3171.
[17] T.A. Zawodzinski, J. Davey, J. Valerio, S. Gottesfeld, Electrochim. Acta 40 (1995) 297.
[18] A.C. West, T.F. Fuller, J. Appl. Electrochem. 26 (1996) 557.
[19] D.M. Bernardi, M.W. Verbrugge, J. Electrochem. Soc. 139 (1992) 2477.
[20] R.B. Bird, W.E. Stewart, E.N. Lightfoot, Transport Phenomena, Wiley, New York, 1960.
[21] F.P. Incropera, D.P. DeWitt, Fundamentals of Heat and Mass Transfer, Wiley, New York, 1996.